Li, Feitao; Oliva Ramírez, Manuel; Wang, Dong; Schaaf, Peter

Effect of SiO2 interlayer thickness in Au/SiO2/Si multilayer systems on Si sources and the formation of Au-based nanostructures

Original published in:	Advanced materials interfaces. - Weinheim : Wiley-VCH. - 9 (2022), 2, art. 2101493, 9 pp.
Original published:	2021-12-02
ISSN:	2196-7350
DOI:	10.1002/admi.202101493
[*Visited:*	2023-03-16]

ADVANCED MATERIALS INTERFACES
www.advmatinterfaces.de

Effect of SiO_2 Interlayer Thickness in Au/SiO_2/Si Multilayer Systems on Si Sources and the Formation of Au-Based Nanostructures

Feitao Li, Manuel Oliva-Ramírez, Dong Wang,* and Peter Schaaf*

Si sources involved in the growth of Au–SiO_x nanostructures are investigated through the rapid thermal annealing of gold thin films on SiO_2/Si substrates with various SiO_2 layer thicknesses (3, 25, 100, 500 nm) in a reducing atmosphere. This method reveals three Si sources whose involvement depends on the thickness of the SiO_2 layers, i.e., Si diffusion from the substrate, and SiO from SiO_2 decomposition and from Si active oxidation. Increasing thicknesses of the SiO_2 layer hampers the Si diffusion and the decomposition of regions of the SiO_2 layer, which decreases the concentrations of discovered regions weakening the Si active oxidation. These discovered regions appear in systems with a SiO_2 layer of 25 or 100 nm, while they are absent for a 500 nm layer. Furthermore, Au–SiO_x nanostructures of different shapes form in each system. Both behaviors indicate that the influence and transport mechanisms of the different Si sources are largely dependent on the thicknesses of the SiO_2 layers and that they control the evolution of the Au–SiO_x nanostructures. A clear understanding of the relationship between these thicknesses and the possible Si sources and their roles in the evolution of the nanostructures makes the tailored fabrication of nanostructures possible.

1. Introduction

In the past decades, both the local surface plasmon resonance (LSPR) of gold (Au) nanoparticles and photoluminescence (PL) emission of silicon oxide (SiO_x) have been widely studied,[1] finding applications in diverse fields such as catalysis, energy conversion and light emission.[2] The combined synthesis of Au–SiO_x nanostructures is a fascinating topic because of the coupling effect between the LSPR of Au nanoparticles and the PL emission of SiO_x, which can enhance and tune their optical properties. In the cases of Au–SiO_x nanoflowers and Au–silica (SiO_2) core–shell structures, that coupling effect leads to an enhancement of the PL emission of the systems.[3] Additionally, Au–SiO_2 core–shell nanoparticles show a wide tunability of LSPR as a function of the thickness of the SiO_2 nanoshell.[4] Therefore, the tailored design of the shape and composition of Au–SiO_x nanostructures is crucial for their functional properties, and the development of an easy-to-control way is indispensable for the final applications.

Au–SiO_x nanostructures are usually synthesized in chemical solutions, which not only makes the final products difficult to control, but also harms the environment.[3b,4] On the contrary, physical routes provide well-controlled and environmental friendly methods to synthetize Au–SiO_x nanostructures.[3a,5] In one of those works, a Au thin film was firstly deposited on a SiO_2/Si substrate and heated up to high temperatures, then the dewetted Au nanoparticles served as the catalyst and the active oxidation of the uncovered Si substrate ($2Si+O_2 \rightarrow 2SiO_{(g)}$, $SiO_{(g)}$ states for SiO in gas form) provided the Si source.[3a] Eventually, the SiO_x nanowires (NWs) nucleated and grew along the surface of the Au nanoparticles based on the vapor-liquid–solid (VLS) mechanism.[6] In this case, the active oxidation of Si only happened within the areas whose SiO_2 layer was etched by Au nanoparticles, which indicated that the thickness of the intermediate SiO_2 layer played an important role in the process. There are also some examples indicating the role of this intermediate SiO_2 layer on controlling the Si diffusion in our previous work. For example, silicide particles form due to the diffusion of Si from the substrate when the intermediate SiO_2 layer is not thick enough (20 nm at above 800 °C),[7] and only solid state dewetting (SSD) of Au–Ag bi-layers occurs in the case of a thicker SiO_2 layer (200 nm at 900 °C).[8] The diffused Si can also help to fabricate SiO_x NWs with the assistant of Au nanoparticles based on solid–liquid–solid (SLS) mechanism.[9] In addition, the decomposition of SiO_2 ($Si+SiO_2 \rightarrow 2SiO_{(g)}$) had been reported,[10] and its product, volatile SiO, can also act as a potential Si source for the growth of SiO_x NWs.[3a] This decomposition reaction happens at a high temperature and within an oxygen-deficient environment,[10] and a reducing ambient of Argon (Ar) and hydrogen (H_2) has also been proved to activate

F. Li, M. Oliva-Ramírez, D. Wang, P. Schaaf
Chair Materials for Electrical Engineering and Electronics
Institute of Materials Science and Engineering and Institute of Micro- and Nanotechnologies MacroNano
TU Ilmenau
Gustav-Kirchhoff-Strasse 5, 98693 Ilmenau, Germany
E-mail: manuel.oliva-ramirez@tu-ilmenau.de; dong.wang@tu-ilmenau.de

The ORCID identification number(s) for the author(s) of this article can be found under https://doi.org/10.1002/admi.202101493.

DOI: 10.1002/admi.202101493

the decomposition reaction because the H_2 can decrease the concentration of oxygen in the atmosphere.[11] Besides, the amount of produced SiO can also be controlled by the thickness of SiO_2 layer. Consequently, a straightforward and high-efficient way to control the proportions of different Si sources consists of using precursors Au thin films onto SiO_2/Si substrates and tuning the thickness of this SiO_2 intermediate layer. Although different intermediate SiO_2 layers have been reported, a study on the different Si sources and their effects on the formation of nanostructures is still absent.[12] Therefore, it is the aim of the present work to unravel the possible Si sources by changing the intermediate oxide layers and their influencing factors on the nanostructures, and finally, achieve the tailored formation of Au–SiO_x nanostructures.

In the present work, four Au/SiO_2/Si systems with different SiO_2 layer thicknesses (3, 25, 100, 500 nm) were thermally annealed at 1050 °C in a reducing atmosphere to produce several nanostructures. Although some of these nanostructures have been reported in scattered works,[3a,5,13] our systematic studies controlling the thickness of the SiO_2 layers identify the roles of three Si sources (SiO from the active oxidation of Si substrate, Si diffusion from the substrate, and SiO from the decomposition of SiO_2 layer) and their transporting mechanisms in each case. This way, in the 3 nm system these three Si sources exist but Si diffusion prevails and hillocks form. In the 500 nm system, for its part, SiO from weak decomposition serves as the only Si source and nanoflowers with shorter NWs can be found. In the intermediate systems with 25 and 100 nm however, the interplay of the different Si sources is more complicated and their synergic combinations result in more nanostructures in both systems. Although the formation of hillocks inside the decomposed areas can be observed in both systems, in the 25 nm system, the enrichment of Si provided by the three Si sources enhances the nucleation of SiO_x NWs and leads to the formation of nanogarlics, and besides, the volatile SiO makes NWs grow from a small part of the bases of the nanogarlics and transform them to nanosprouts. By contrast, in the 100 nm system Si sources from decomposition and active oxidation enable the formation of nanoflowers with longer NWs. The morphologies and compositions of these nanostructures were characterized, and different evolution mechanisms were schematically proposed to explain their formation based on the possible Si sources in each system.

2. Results

2.1. Au–SiO_2-3 System

Figure 1 shows the SEM and EDS results of the 3 nm SiO_2 sample. In Figure 1a, the system Au–SiO_2-3 exhibits large microstructures in the shape of hillocks of about 1.0 µm. According to their material contrast, the bright grey areas should be rich in Au. The larger overview included in the upper inset of Figure 1a does not show special features and the tilted view in the bottom inset confirms that these large microstructures present the shape of hillocks. The cross-sectional view of Figure 1b shows that these hillocks sink into the substrate whereas the area around remains unchanged. The distribution of elements across the hillock of Figure 1c, presented in Figure 1d, exhibits that the bright grey areas are Au rich and the increasing overall concentration of Au towards the center corresponds with the lentil-like shape of the hillocks. Regarding the dark areas, it is difficult to determine their composition since part of the Si signal belongs to the substrate and oxygen offers a low accuracy by EDS. The XRD pattern of Au–SiO_2-3 in Figure S1 in the Supporting Information indicates that all reflexes can be well indexed by fcc-Au.[14] There are also much smaller nanoparticles distributed among the above-mentioned hillocks, as shown in Figure 1a. The detailed morphologies and compositions of several of these smaller nanoparticles are shown in Figure S2 in

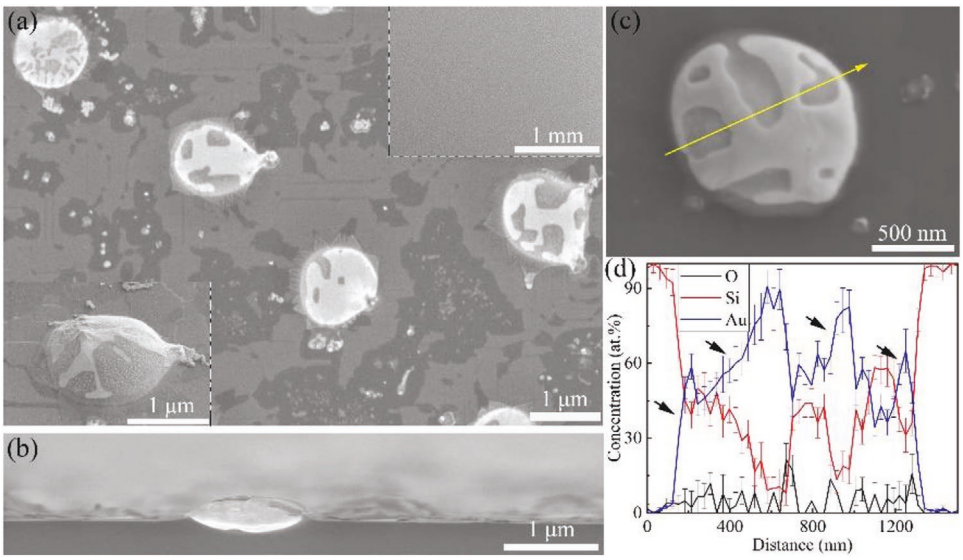

Figure 1. Morphologies and element distributions in Au–SiO_2-3. a) Top-view SEM image. The upper inset shows a large overview and the bottom inset is the tilted view of one hillock. b) Cross-sectional view SEM image. c) Top-view SEM image of a selected hillock. d) Element distribution obtained by EDS line scanning along the yellow arrow that cross the hillock in (c). The arrows in (d) mark the increasing concentration of Au corresponding to the bright grey areas in (c).

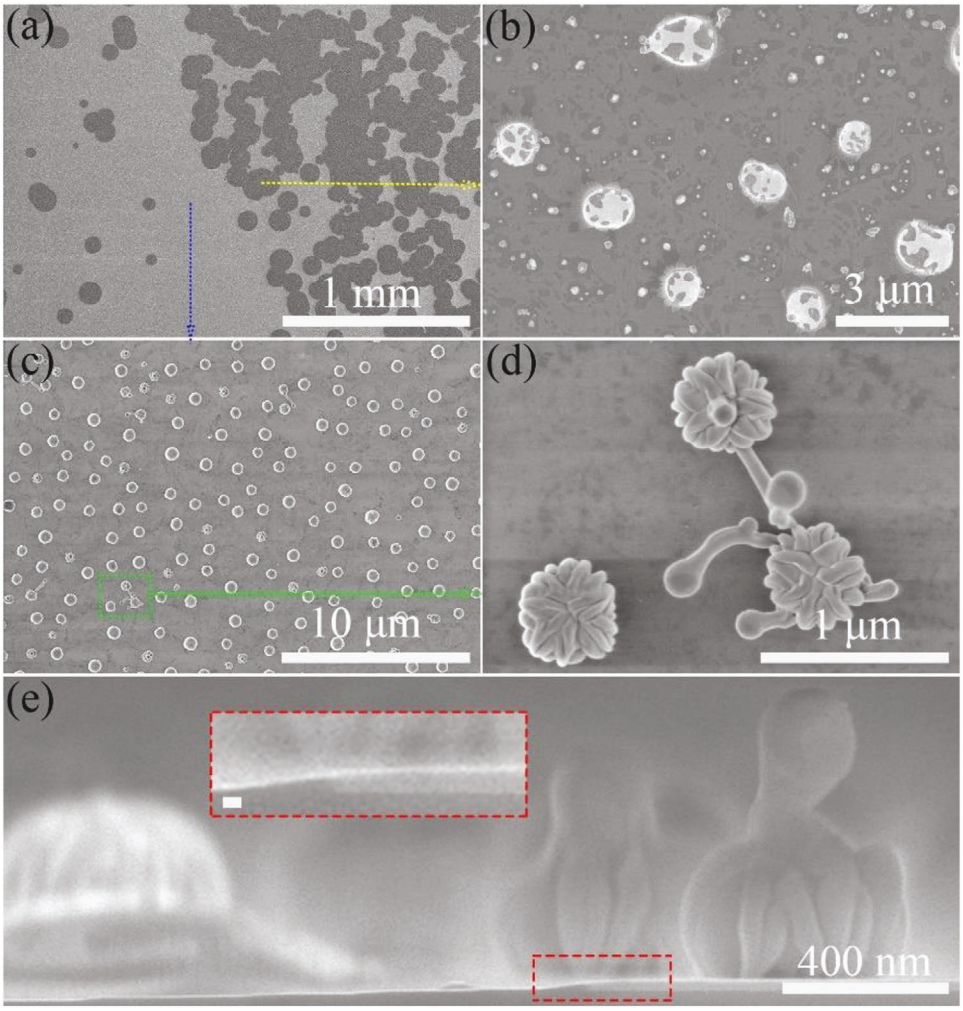

Figure 2. Selected characteristic nanostructures present in the Au–SiO_2-25. a) Large SEM overview. The details in the dark areas are enlarged in (b) and the details in the grey areas are enlarged in (c). d) High-magnification image of nanostructures squared in green square in (c). e) Cross-sectional view of both dark area (left) and grey area (right). The inset is the enlargement of the junction between the two areas. (Scale bar of inset: 20 nm).

the Supporting Information, where these particles also show the presence of Au and contrast of two compositions. Therefore, the formation mechanism of smaller nanoparticles should be similar to that of the larger hillocks.

2.2. Au–SiO_2-25 System

The system Au–SiO_2-25 in **Figure 2** presents hillocks too but also nanostructures with completely different morphologies. The large overview in Figure 2a shows two distinct areas, single or merged dark areas with a nearly circular shape, and grey regions. Figure 2b shows that these dark areas present hillocks, and Figure 2c displays another two kind nanostructures in the grey regions. The further enlarged image of this section in Figure 2d exhibits that most of the motifs of Figure 2c present a dendritic surface with many interlacing NWs, which confer them a garlic-like morphology and so, we will refer to them as nanogarlics. Besides, a few nanogarlics present several NWs growing from them with a nanoparticle on top, looking like a sprout and we will refer to them as nanosprouts. The cross-sectional view of a junction between dark and grey regions in Figure 2e shows that the SiO_2 layer still exists in the grey area and that it disappears in the dark area leaving a slight depression. The absence of the SiO_2 layer in this region can be attributed to the decomposition reaction between the SiO_2 layer and the Si substrate because the etching effect of H_2 on the SiO_2 layer cannot decompose it as it was shown in our previous work.[11] The lateral views of two nanosprouts formed onto the SiO_2 layer clearly detail the dendritic structures from their bottom. The hillocks formed inside the dark areas in this system also sink into the substrate as in Au–SiO_2-3, as shows Figure S3 in the Supporting Information.

The EDS line scans in **Figure 3**a,b shows that the bright grey areas of the hillocks formed in Au–SiO_2-25 are Au-rich as in Au–SiO_2-3. Furthermore, the XRD diagram in Figure S1 in the Supporting Information indicates the existence of pure Au in Au–SiO_2-25. The two plateaus of the composition line of oxygen in Figure 3d correspond to the sides of the nanogarlic in Figure 3c, and they indicate that its outer

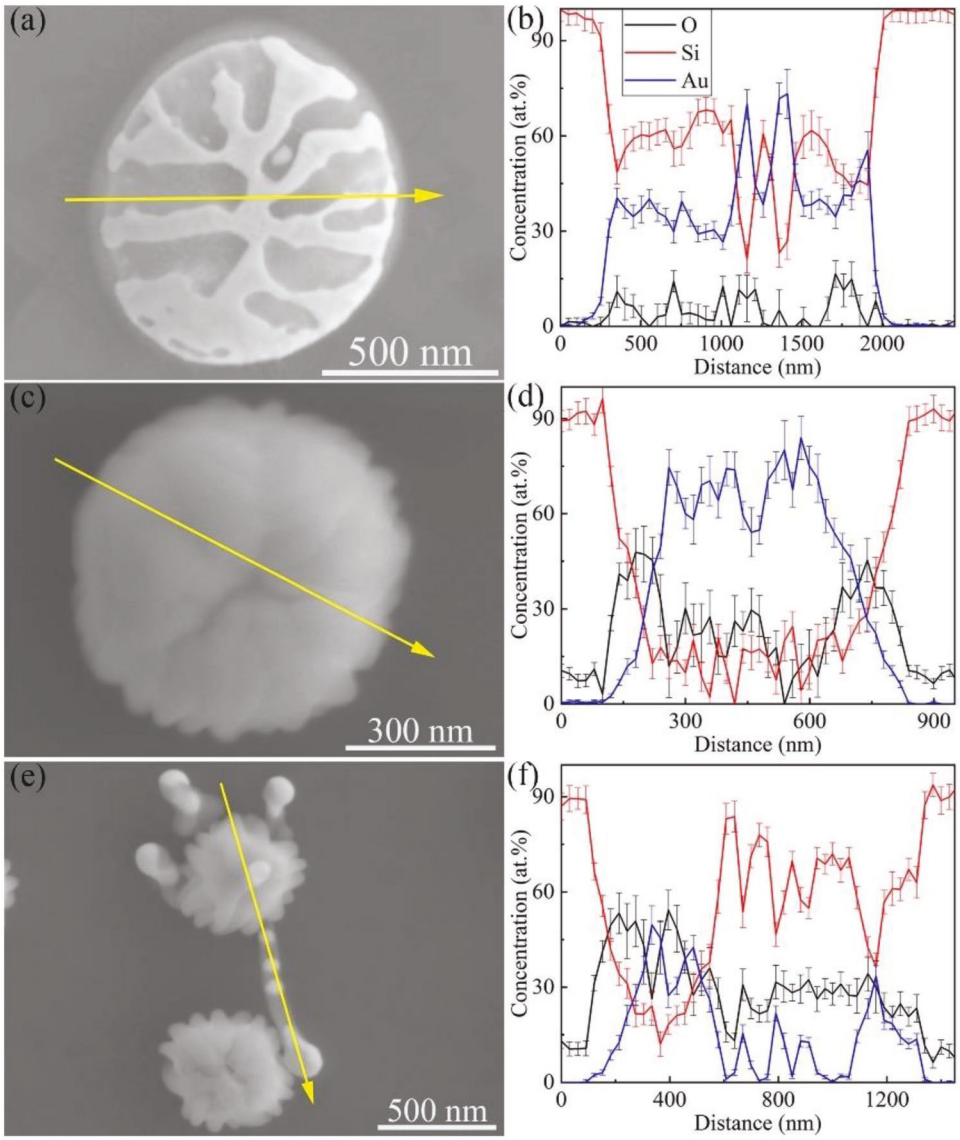

Figure 3. EDS measurements of selected characteristic nanostructures of the Au–SiO_2-25. The element distributions in (b,d,f) were recorded along the arrows in (a,c,e), respectively. The legend in (b) is also valid for (d,f).

layer should be SiO_x, meaning that the nanogarlics present a Au–SiO_x core–shell structure. The nanosprout in Figure 3e shows several isolated nanoparticles within the long nanowire, and element distributions in Figure 3f indicate that the bottom part of the nanosprout presents similar element distributions than that of the nanogarlic, i.e., an outer layer of SiO_x and a core of Au. Besides, both top nanoparticles and inside nanoparticles consist of Au.

2.3. Au–SiO_2-100 and Au–SiO_2-500 Systems

Figure 4a shows that the Au–SiO_2-100 also presents two different areas although the concentration of dark regions is much lower than that in the Au–SiO_2-25. In those dark areas, the hillocks formed again and in the grey area appear microstructures consisting of nanoparticles surrounded by NWs, which make the whole structure presents a flower-like morphology that we labeled as nanoflower. For a better visibility of the NWs, only one nanoparticle or nanoflower is shown in the insets. Larger overviews of the hillocks and the nanoflowers are shown in Figure S4 in the Supporting Information. The cross-sectional view of Figure 4b shows that the dark areas in Au–SiO_2-100 are concave cavities, which means that not only the SiO_2 layer of the cavities disappears, but also part of the Si substrate is consumed. Similarly, the absence of SiO_2 layer results from the decomposition of the SiO_2 layer as it happened in Au–SiO_2-25. In the Au–SiO_2-500, for its part, there is no visible dark regions from the large overview of Figure 4c, and only nanoflowers can be observed over the whole sample. These nanoflowers, as shown in the inset of Figure 4c, present shorter surrounding NWs than those of Au–SiO_2-100. Figure S5 in the Supporting Information shows one lateral-view image outside the dark regions in Au–SiO_2-100 and a lateral-view image in Au–SiO_2-500,

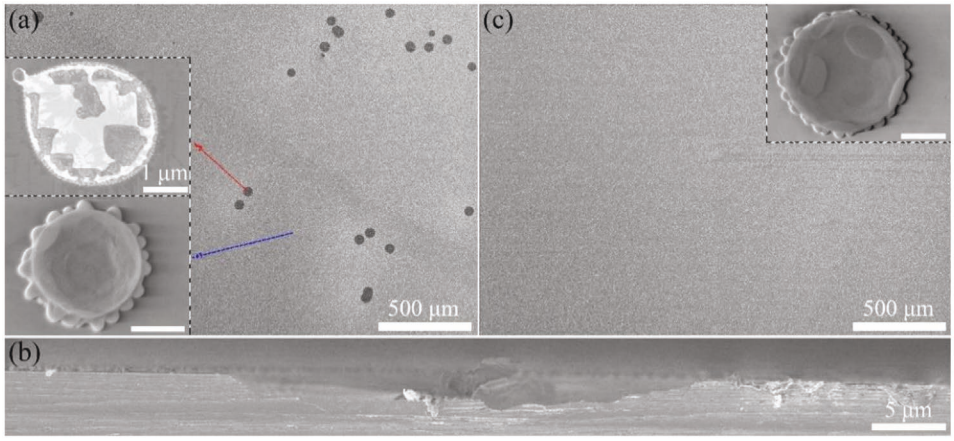

Figure 4. a) Top-view SEM image of system Au–SiO_2-100. A selected characteristic hillock and nanoflower from the dark and grey areas are enlarged in the upper and lower insets, respectively. b) Cross-sectional SEM view across a dark area of Au–SiO_2-100. c) Top-view SEM image of Au–SiO_2-500. The inset shows a characteristic nanoflower of this sample. The scale bars for both nanoflowers in the insets measure 200 nm.

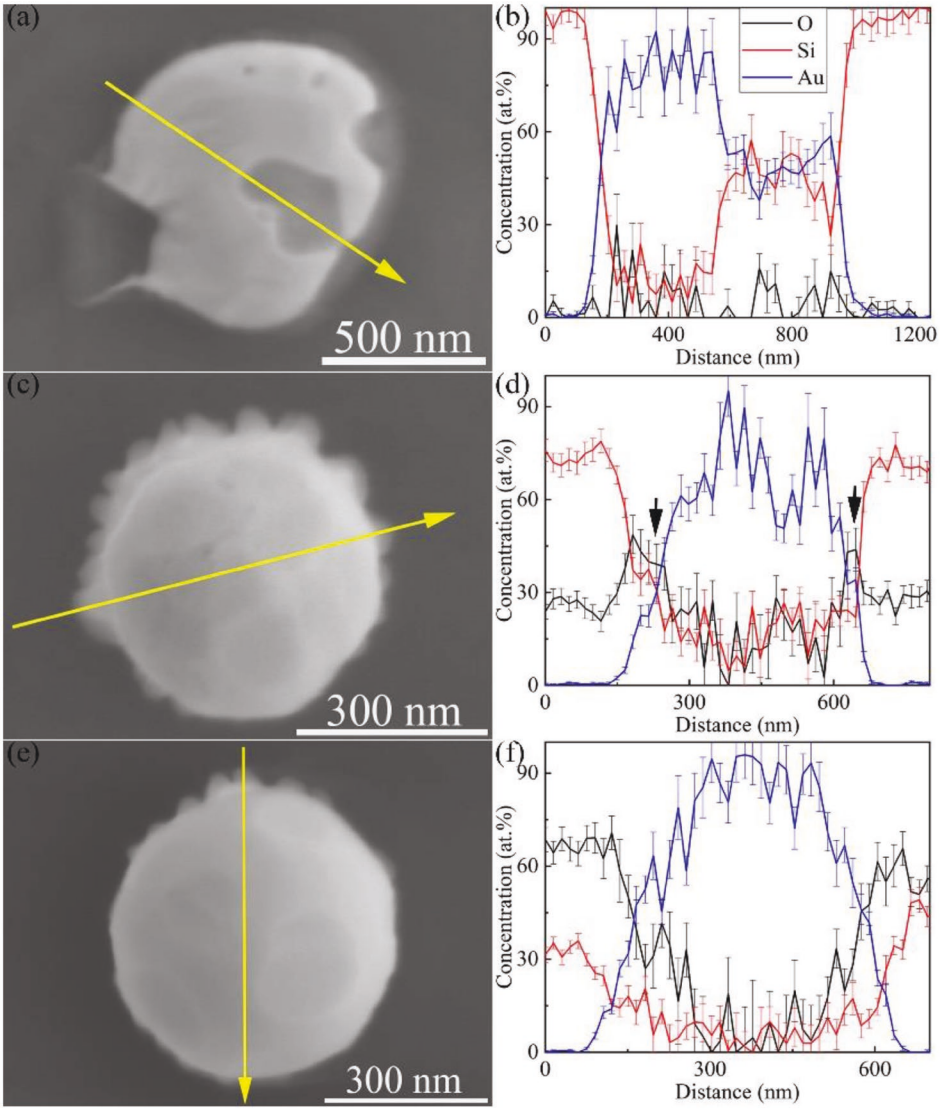

Figure 5. EDS measurements of selected characteristic nanostructures of a–d) Au–SiO_2-100 and e,f) Au–SiO_2-500. The element distributions in (b,d,f) were recorded along the arrows in (a,c,e), respectively. The legend in (b) is also valid for (d,f). The regions marked by arrows in (d) correspond to NWs.

which do not show any special features such as hillocks or cavities.

The EDS line scans in **Figure 5**b,d shows that in Au–SiO_2-100 both the bright grey areas of the hillocks and the central nanoparticle of the nanoflowers are Au-rich. Besides, the plateaus of the lines of Si and oxygen corresponding to the NWs in Figure 5d mean that the composition of these NWs might be SiO_x. The EDS scan of a nanoflower of Au–SiO_2-500 in Figure 5f shows that it presents a Au-rich central particle too. Regarding its surrounding NWs, the scan does not show any clear composition because of their short length but it is reasonable to believe they are made of SiO_x as the NWs of the Au–SiO_2-100. The XRD diffractograms of Au–SiO_2-100 and Au–SiO_2-500 in Figure S1 in the Supporting Information show reflexes that can be well identified as Au for both samples and there is also a weak reflex belonging to Au silicide in the Au–SiO_2-100.[11,15]

3. Discussion

The morphologies and compositions of the nanostructures formed in the four systems show that the thickness of the intermediate SiO_2 layer plays a crucial role in tailoring the finally obtained nanostructures. Among them, similar hillocks can be found in Au–SiO_2-3, Au–SiO_2-25 and Au–SiO_2-100, and the concentration of dark areas with hillocks decreases with the increasing thickness of the SiO_2 layer. Nanogarlics and nanosprouts occur in Au–SiO_2-25 while nanoflowers form in Au–SiO_2-100 and Au–SiO_2-500. The following schematic diagrams will be introduced to explain systematically the formation of the different microstructures based on the possible Si sources and their transport mechanisms in each system.

3.1. Formation of Hillocks and Nanoflowers

Similar hillocks have been reported on both (111) and (100) Si substrates.[13] At 1050 °C, in Au–SiO_2-3 several processes such as the SSD of Au thin film,[16] the decomposition of native SiO_2 layer,[10a,17] the active oxidation of exposed Si substrate after decomposition of SiO_2,[3a] and the interdiffusion of Au/Si,[13c] might take place. Despite we cannot determine the sequence of these processes, the thin SiO_2 layer and the lack of clear depressions in Figure 1b indicate that the Au/Si interdiffusion dominates in this system,[17] and that the sinking of the hillocks in Figure 1b originates from such interdiffusion. Because the annealing temperature was much higher than the eutectic point, it can be imagined that the formation of the hillocks was related to the eutectic transitions locally during the heating and cooling stages. Au–Si liquid droplets form at high temperature, and their phase separation initiates during the cooling period forming hillocks with two different contrasts.[13a,b] It is reasonable to see the formation of hillocks in Au–SiO_2-3 because such thin oxide layer cannot effectively hinder the interdiffusion at high temperature. However, this formation is not that intuitive in Au–SiO_2-25 and especially in Au–SiO_2-100, where the SiO_2 should act as an effective blocking layer. Some metal atoms can diffuse through SiO_2 blocking layers assisted by existing microchannels to the SiO_2/Si interface,[18] which might also happen in our case. In addition, the circular shape and the heterogeneous distribution of dark cavities observed in Figures 2a and 4a further prove the existence of the SiO_2 decomposition in Au–SiO_2-25 and Au–SiO_2-100.[10a,11]

To bring to light and quantify the etching effect of H_2 in the SiO_2 layer, Figure S6 in the Supporting Information gives a group of reference experiments for samples without Au thin film on top. After annealing in the reducing environment, some scattered special areas can be found on the surfaces of SiO_2-3 and SiO_2-25. By contrast, there are no visible features in the other two samples. The absence of any features in SiO_2-100 and SiO_2-500 can also exclude the existence of H_2 etching effect on the SiO_2 layer, which agrees with our previous work.[11] Those special areas in SiO_2-3 and SiO_2-25 come from the SiO_2 layer decomposition, and these results show how increasing the thicknesses of SiO_2 layers hinder gradually the SiO_2 decomposition. Besides, the few decomposed areas in the reference experiments compared with the samples covered by Au thin films also prove that the Au atoms can diffuse to the SiO_2/Si interface enhancing the SiO_2 decomposition there.

Figure 6 presents schematic diagrams of the formation of hillocks and nanoflowers. At the initial stage of the annealing, apart from the SSD of the Au thin film, the diffusion of Au from the thin film to the interface SiO_2/Si through defects (dashed lines) begins, as shown in Figure 6a. Simultaneously, the decomposition reaction initiates at the interface and it can be strengthened by the diffused Au. In turn, the resulted holes from the decomposition provide the places for the formation of hillocks, as shows Figure 6b. The decomposed areas (holes) keep growing laterally and piercing vertically the SiO_2 layer to the surface of Si.[10a,18b] Those nanostructures (nanogarlics and nanosprouts in Au–SiO_2-25 and nanoflowers in Au–SiO_2-100) that formed on the oxide layer (outside the cavities) will drop into the cavities and contact with the exposed Si substrate, as indicates the blue arrows in Figure 6c. There, their outer SiO_x reacts with Si based on the decomposition reaction, and the remaining Au precipitates in the formation of Au–Si liquid droplets and then hillocks form upon cooling due to the phase separation (Figure 6d). Within the cavities formed in Au–SiO_2-100 (Figure 6c), the formed hillocks present a random size distribution in the inner part of the cavities and much larger sizes close to their borders. Such distribution has been also reported in our previous research.[11] However, the size distribution of hillocks in the cavities of Au–SiO_2-25 is random everywhere, as shows in Figure S7 in the Supporting Information. This difference may respond to the expansion rate of the cavities during their formation. When the cavities form, those Au–Si droplets near the borders tend to diffuse to favored positions where they can have lower energies due to the geometric local negative curvature based on the Gibbs-Thomson effect,[16b] and they will agglomerate with each other. As the cavities keep expanding during the annealing process, the droplets move together with the border because there they have the lowest energy. During the movement, the droplets lose material in the shape of smaller droplets that transform to hillocks with random sizes upon cooling. The results in Figures 2a and 4a indicate that the cavity expansion rate in Au–SiO_2-100 is much slower than that in Au–SiO_2-25. Therefore, compared with Au–SiO_2-25, the droplets in Au–SiO_2-100 can easier catch up with the border expansion.

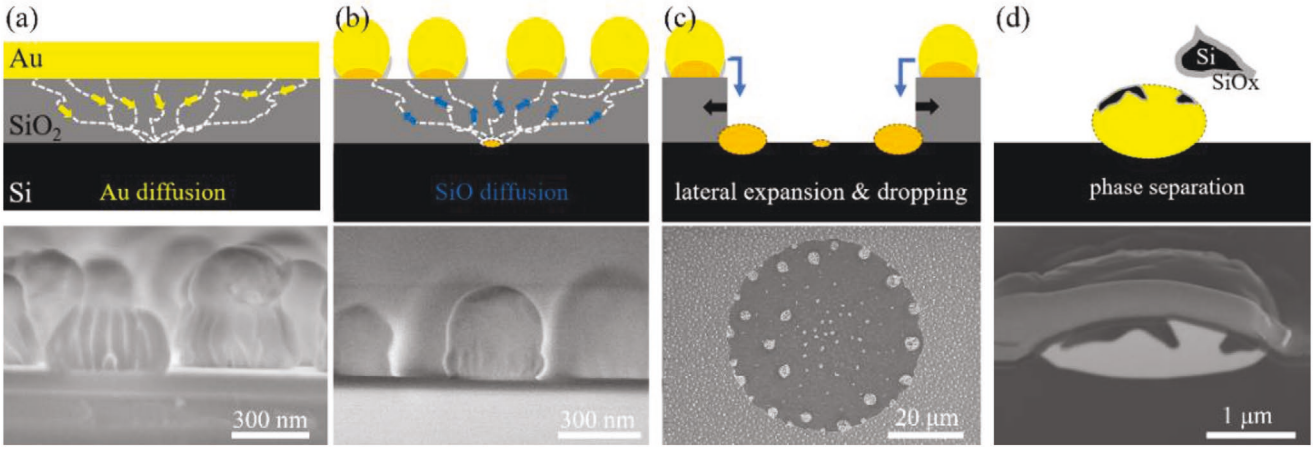

Figure 6. Formation mechanisms of hillocks and nanoflowers in Au–SiO_2-25/100/500 systems. a) Au diffusion. b) SiO diffusion. Nanoflowers in Au–SiO_2-100 (left) and Au–SiO_2-500 (right), respectively. c) Lateral expansion of the cavity and absorption of Au from dropping nanostructures. Image of a full cavity area in Au–SiO_2-100. d) Phase separation in the decomposed areas. The enlargement shows the clearer core–shell structure for separated dark areas. The image is FIB-cutting cross section of a hillock in Au–SiO_2-25. The yellow color represents Au and the orange color means the formation of Au–Si.

Furthermore, the border droplets in Au–SiO_2-100 can absorb more Au from the dropping nanostructures and their sizes become larger with the expansion. Such growth in size of the border hillocks with the annealing time was also observed in our previous work.[11] In contrast, in Au–SiO_2-25, the droplets of the border cannot follow the expansion of the cavities due to its faster growth rate. This way, these border droplets cannot absorb more Au from the dropping nanostructures before they left the expanding border. Therefore, the hillocks do not present large sizes at the border of the cavities in Au–SiO_2-25 as shows in Figure S7 in the Supporting Information. The cross-sectional image of a hillock in Figure 6d reveals a dark phase distributed within the upper part of the hillock covered by a very thin layer. Combine with the above EDS results, the bright areas are Au while the dark areas are Si covered by a thin layer of SiO_x. This result suggests that the separated Si phase tends to agglomerate and only the Si at the interphases and surface can be oxidized. By this means, the hillocks form in the decomposed areas of Au–SiO_2-25 and Au–SiO_2-100 systems, as shown in Figures 2b and 4a.

Similar flower-like nanostructures had been reported and the authors attributed the Si source of surrounding SiO_x NWs to the active oxidation of the Si substrate.[3a] That mechanism might be valid for Au–SiO_2-100 because it presents large depressed cavities (Figure 4b), which can only be the result of active oxidation. However, the sample surface of Au–SiO_2-500 in Figure 4c does not show any cavities, which means that the Si substrate is fully covered by the SiO_2 layer and the active oxidation of Si cannot take place. The diffusion of Au to the interface shown in Figure 6a has been proved to be able to enhance the decomposition.[11,18] However, the extremely thick SiO_2 layer in Au–SiO_2-500 can largely slow down the Au diffusion and the enhancement effect of the diffused Au is not so effective, leading to the absence of cavities in this sample. Since the Si cannot diffuse across the 500 nm SiO_2 layer within one minute,[19] the only conceivable Si source may come from the decomposition at the Si/SiO_2 interface. Figure 6b schematically shows how the formed SiO gas can be transported to the surface through the defects in the SiO_2 layer (dashed lines), and precipitates giving rise to nanoflowers. The longer length of the surrounding SiO_x NWs of nanoflowers in Au–SiO_2-100 than those in Au–SiO_2-500, as shown in the lateral views of Figure 6b, can be attributed to the different amount of Si received in each case. The Au in Au–SiO_2-100 can diffuse more quickly to the interface and enhance the decomposition rate producing more SiO gas in this system. Moreover, in Au–SiO_2-100 there is a second Si source from the active oxidation of the uncovered Si inside the cavities.

3.2. Formation of Nanogarlics

As the dark cavities in Figure 2a come from the decomposition of the SiO_2 layer, volatile SiO from the decomposition can act as a Si source in Au–SiO_2-25. The lateral image in Figure 2e also shows a slight depression inside the cavity regions, which indicates that the active oxidation of uncovered Si happens and provides volatile SiO as another Si source. Besides, contributions of Si diffusion from the substrate should be considered because they have been reported in a similar system after annealing at 800 °C.[7] Therefore, three Si sources might exist in Au–SiO_2-25.

Figure 7 presents the formation mechanism of the nanorgarlics in Au–SiO_2-25. In this system, the initial stages such as the SSD of the Au thin film and the diffusion of Au and SiO gas are analogous to those described in Figure 6a,b for the formation of nanoflowers. Then the discussion begins at the stage shown in Figure 7a where three Si sources are marked. With abundant Si supplies, central particles of nanoflowers quickly and fully transform to Au–Si droplets and new NWs nucleate and grow on the surface of the droplets, as shows in Figure 7b. Different growth directions of these NWs along the surface produce the dendritic morphology exhibited in Figure 2. Some NWs even grow into the droplet because the original growth directions are prevented by other NWs, as shown in Figure 7c. During the phase separation period of Figure 7d, the Si of droplets tends to nucleate attaching to the inserted SiO_x NWs forming a thin Si layer which can be oxidized to SiO_x, as proved by the FIB-cutting results in Figure 7e. Since one Si source is from the diffusion (solid) and another two are from the active oxidation and decomposition

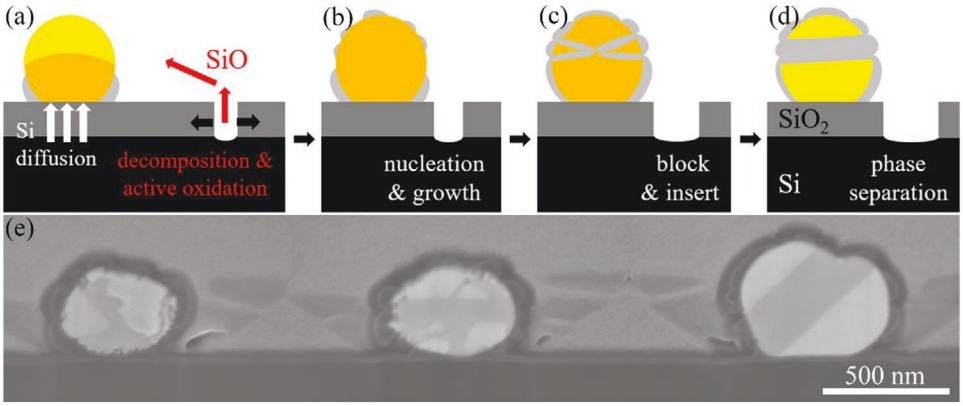

Figure 7. Formation mechanism of nanogarlics in Au–SiO_2-25. Schematic diagrams at different stages: a) possible Si sources, b) nucleation and growth of new NWs, c) block and insert of NWs, d) phase separation. e) FIB-cutting cross sections of some nanogarlics. The yellow color represents Au and the orange color means the formation of Au–Si.

(vapor), both SLS and VLS mechanisms contribute to the growth of NWs in this system. As for the occurrence of nanosprouts, it should be highly related to volatile SiO because the nanoparticle on each nanowire of nanosprouts in Figures 2d and 3e is a typical feature for the VLS mechanism.[6] However, the decomposition proceeds fast because of the thin oxide layer, and the active oxidation is not obvious due to the slight depression in Figure 2e. These factors make difficult to determine the origin of nanosprouts. Therefore, a systematic formation mechanism of nanosprouts has be elaborated in another work by using a thicker SiO_2 layer and different annealing times and their formation can be attributed to the direction change of the main SiO source.[11] As for the nanoparticles inside one nanowire in Figure 3e, this kind of structure can be attribute to Rayleigh instabilities driven by the surface free energy of the coated Au rich core or diffusion processes of the Au tip.[20] Once the nanoparticle formed inside the nanowire, it becomes another catalyst site for the growth of new NWs and that is the reason of branched growth of NWs in Figure 2d.

4. Conclusions

In the present work, we have fabricated several nanostructures by RTP annealing under a reducing atmosphere by changing the thickness of a SiO_2 layer between a Au thin film and the Si (100) substrate. SiO_2 decomposition happens in all cases due to the appropriate annealing parameters, and it becomes more hindered with increasing the SiO_2 thickness. Similarly, Si diffusion can be prevented by increasing the SiO_2 thickness. The thin SiO_2 layer in Au–SiO_2-3 and the SiO_2 decomposition in Au–SiO_2-25 and Au–SiO_2-100 provide suitable situation for the interdiffusion of Au and Si, which favors the formation of hillocks consisting of separated phases of Au and Si–SiO_x core–shell structures upon cooling.

On the remained SiO_2 layer, the formation of different nanostructures can be controlled by different Si sources allocated by SiO_2 layer thickness. The thin SiO_2 layer in Au–SiO_2-25 allows the Si diffusion, the Si active oxidation, and the SiO_2 decomposition providing abundant Si sources, which enhances the nucleation of SiO_x NWs and leads to the formation of Au–SiO_x core–shell nanogarlics with dendritic morphology. Besides, volatile SiO from Si active oxidation and SiO_2 decomposition enables several SiO_x NWs to grow from the bases of nanogarlics and to evolve to nanosprouts. The thick SiO_2 layers in Au–SiO_2-100 and Au–SiO_2-500 can prevent Si diffusion but the SiO_2 decomposition in Au–SiO_2-100 is faster, producing more volatile SiO and introducing another Si source from active oxidation, and finally result in longer NWs of nanoflowers in Au–SiO_2-100.

Unraveling the role of the different Si sources acting in the systems due to the thickness of their SiO_2 layers allows tailoring the formation of different nanostructures by tuning the thickness of the oxide layer. This study also provides further details on the diffusion of Au and volatile SiO in the SiO_2 layer, which may be useful in Au-assisted growth of NWs, especially in the case of Si substrate with a thick oxide layer.

5. Experimental Section

Substrates Preparation and Thin Film Deposition: Four inch single-side polished p-type (100) oriented Si-wafers (5–10 Ω cm) with SiO_2 layers of four different thicknesses (3, 25, 100, and 500 nm) were used as substrates. The wafers presented a native oxide layer of 3 nm, and the SiO_2 layers of 25, 100, and 500 nm for the other cases were thermally grown. The as-received wafers presenting this native oxide layer were used for the Au–SiO_2-3 system. Before the fabrication of the samples for the other systems, the native oxide layers of the as-received wafers were removed with hydrofluoric acid and then, SiO_2 layers of the scheduled thicknesses were thermally grown. These Si wafers were then cut into small square pieces of 10 × 10 mm^2 that were cleaned with acetone and isopropanol followed by rinsing deionized water. A 20 nm thick Au film was then deposited on these substrates by using electron beam evaporation (CS400ES, VON ARDENNE). The deposition was carried out at room temperature under a base pressure of 1×10^{-6} mbar and their thicknesses were controlled by a quartz microbalance.

Thermal Processing: Rapid thermal processing (RTP, Jipelec 100) of the samples was carried out at 1050 °C and the annealing was independently conducted for each sample. The chamber was evacuated and purged with Ar several times. Gas flows of 1500 sccm of Ar and 50 sccm of H_2 were kept during the whole annealing process. The annealing process consisted of heating up to 1050 °C from room temperature within 20 s, and annealing for 1 min. Then, the heating was switched off leading to a fast cooling. Figure S8 in the Supporting Information shows the temperature profile measured by the pyrometer of the RTP system. The samples were labeled as Au–SiO_2-3, Au–SiO_2-25, Au–SiO_2-100, and Au–SiO_2-500 based on the thickness of the SiO_2 layer. Bare SiO_2/Si substrates with SiO_2 layers of 3, 25, 100, and 500 nm were also treated

by RTP using the same annealing parameters than those used for the samples covered by Au thin films. An analogous nomenclature, SiO_2-3, SiO_2-25, SiO_2-100, and SiO_2-500, was used to refer to them.

Characterization: The samples were characterized by high-resolution scanning electron microscopy (HR-SEM, Hitachi S-4800) and top- and lateral-view images were recorded. The SEM images were recorded by using mixed signals from secondary electrons and back scattered electrons (BSE) to minimize charging effects due to the bad electrical conductivity of the SiO_2 layer. Besides, the composition information related to Z-contrast was obtained with the BSE detector because the areas which are rich in elements with higher atomic number show brighter contrast. Energy-dispersive X-ray spectroscopy (EDS, Thermo Scientific) was used to analyze the composition. A focused ion beam (FIB, Zeiss Auriga 60 dual beam) was used to cut some representative nanoparticles of the Au–SiO_2-25 to check their cross-sectional view. Before the FIB cutting, protective carbon and platinum layers were deposited onto the target areas via electron and gallium ion beams. X-ray diffraction (XRD, Siemens D-5000) measurements were carried out at grazing incident diffraction geometry (incident angle: 3°) using Cu-K_α irradiation at 40 kV.

Supporting Information

Supporting Information is available from the Wiley Online Library or from the author.

Acknowledgements

The work was supported by the Deutsche Forschungsgemeinschaft (DFG, grant Scha 632/20, "FunPartY" and grant Scha 632/24, "Tailored Disorder" and Scha 632/27, "DFG-Gerätezentrum"). This work was also supported by the free state of Thuringia under grants 2015 FGI 0025 305 (FastμXRD) and B715-10009 (BioMacroNano2020), all co-financed by the European Union within the framework of the European Regional Development Fund (ERDF). Joachim Döll and Paul Bucklitsch from the Center of Micro- and Nanotechnology (ZMN), a DFG-funded core facility at TU Ilmenau, are acknowledged for their professional help in the preparation of the samples.

Open access funding enabled and organized by Projekt DEAL.

Conflict of Interest

The authors declare no conflict of interest.

Data Availability Statement

The data that support the findings of this study are available from the corresponding author upon reasonable request.

Keywords

Si active oxidation, Si diffusion, SiO_2 decomposition, solid–liquid–solid, vapor–liquid–solid

Received: August 12, 2021
Revised: October 11, 2021
Published online: December 2, 2021

[1] a) W. Li, Q. Jia, X. Liu, J. Zhang, *Ceram. Int.* **2017**, *43*, 2950; b) H. B. Jeon, P. V. Tsalu, J. W. Ha, *Sci. Rep.* **2019**, *9*, 13635; c) Y. Chen, Y. Huang, H. Huang, P. Su, T. Perng, L. Chen, *Nano Energy* **2020**, *67*, 104225; d) N. M. Devi, S. A. Lynrah, R. Rajkumari, N. K. Singh, *Sens. Actuators, A* **2021**, *327*, 112744.
[2] a) Z. Kang, B. Arnold, C. Summers, B. Wagner, *Nanotechnology* **2006**, *17*, 4477; b) C. Zhang, Q. Luo, J. Shi, L. Yue, Z. Wang, X. Chen, S. Huang, *Nanoscale* **2017**, *9*, 2852; c) F. Lei, H. Liu, J. Yu, Z. Tang, J. Xie, P. Hao, G. Cui, B. Tang, *Phys. Chem. Chem. Phys.* **2019**, *21*, 1478; d) M. Oliva-Ramirez, D. Wang, D. Flock, V. Rico, A. R. Gonzalez-Elipe, P. Schaaf, *ACS Appl. Mater. Interfaces* **2021**, *13*, 11385.
[3] a) H. Luo, R. Wang, Y. Chen, D. Fox, R. O'Connell, J. Wang, H. Zhang, *CrystEngComm* **2013**, *15*, 10116; b) Q. Wang, J. Zhang, X. Sang, D. Zhang, Q. Shi, S. Li, W. Wang, *J. Lumin.* **2018**, *204*, 284.
[4] Y. Lu, Y. Yin, Z. Li, Y. Xia, *Nano Lett.* **2002**, *2*, 785.
[5] P. Zhang, Y. Cui, *CrystEngComm* **2013**, *15*, 9963.
[6] a) R. S. Wagner, W. C. Ellis, *Appl. Phys. Lett.* **1964**, *4*, 89; b) B. J. Kim, J. Tersoff, S. Kodambaka, M. C. Reuter, E. A. Stach, F. M. Ross, *Science* **2008**, *322*, 1070.
[7] D. Wang, P. Schaaf, *Phys. Status Solidi A* **2013**, *210*, 1512.
[8] D. Wang, P. Schaaf, *J. Mater. Chem.* **2012**, *22*, 5344.
[9] M. Paulose, O. K. Varghese, C. A. Grimes, *J. Nanosci. Nanotechnol.* **2003**, *3*, 341.
[10] a) R. Tromp, G. W. Rubloff, P. Balk, F. K. LeGoues, E. J. van Loenen, *Phys. Rev. Lett.* **1985**, *55*, 2332; b) K. Hofmann, G. W. Rubloff, R. A. McCorkle, *Appl. Phys. Lett.* **1986**, *49*, 1525; c) K. Hofmann, G. Rubloff, M. Liehr, D. Young, *Appl. Surf. Sci.* **1987**, *30*, 25.
[11] F. Li, M. Oliva-Ramírez, D. Wang, P. Schaaf, *Mater. Des.* **2021**, *209*, 109956.
[12] a) H. Hijazi, F. Leroy, G. Monier, G. Grégoire, E. Gil, A. Trassoudaine, V. G. Dubrovskii, D. Castelluci, N. I. Goktas, R. R. LaPierre, Y. André, C. Robert-Goumet, *J. Phys. Chem. C* **2020**, *124*, 11946; b) A. Rath, J. K. Dash, R. R. Juluri, A. Rosenauer, M. Schoewalter, P. V. Satyam, *J. Appl. Phys.* **2012**, *111*, 064322.
[13] a) B. Ressel, K. C. Prince, S. Heun, Y. Homma, *J. Appl. Phys.* **2003**, *93*, 3886; b) N. Ferralis, R. Maboudian, C. Carraro, *J. Am. Chem. Soc.* **2008**, 2681; c) Y. Shao, T. Nie, Z. Jiang, J. Zou, *Appl. Phys. Lett.* **2012**, *101*, 053104.
[14] H. E. Swanson, *Standard X-Ray Diffraction Powder Patterns*, US Department of Commerce, National Bureau of Standards, MD, USA **1953**.
[15] a) B. Tsaur, J. Mayer, *Philos. Mag. A* **1981**, *43*, 345; b) L. Hultman, A. Robertsson, H. Hentzell, I. Engström, P. Psaras, *J. Appl. Phys.* **1987**, *62*, 3647.
[16] a) D. Wang, P. Schaaf, *J. Mater. Sci.: Mater. Electron.* **2010**, *22*, 1067; b) D. Wang, R. Ji, P. Schaaf, *Beilstein J. Nanotechnol.* **2011**, *2*, 318; c) D. Wang, P. Schaaf, *J. Mater. Sci.* **2011**, *47*, 1605.
[17] T. H. Kim, A. Shalav, R. G. Elliman, *J. Appl. Phys.* **2010**, *108*, 076102.
[18] a) H. Dallaporta, M. Liehr, J. E. Lewis, *Phys. Rev., B Condens. Matter Mater. Phys.* **1990**, *41*, 5075; b) P. Bábor, R. Duda, J. Polčák, S. Průša, M. Potoček, P. Varga, J. Čechal, T. Šikola, *RSC Adv.* **2015**, *5*, 101726.
[19] Z. Yang, Y. Zhang, D. Liu, E. Nie, Z. Jiao, Y. Jin, Y. He, M. Gong, X. Sun, *J. Non.-Cryst. Solids* **2010**, *356*, 2207.
[20] N. H. Fletcher, R. G. Elliman, T. H. Kim, *Nanotechnology* **2009**, *20*, 085613.